Reconfigurable OTA Chamber: A New Paradigm for Testing of MIMO Wireless Devices

Rashid Mehmood, Michael A. Jensen
Electrical and Computer Engineering
Brigham Young University, Provo, UT, USA

Jon W. Wallace
Electrical and Computer Engineering
Lafeyette College, Easton, PA, USA

***Abstract*—Over-the-air testing (OTA) of wireless devices in realistic but repeatable environments is typically performed using either an expensive multi-antenna OTA chamber that provides a high level of multipath control or a low-cost mode-stirred reverberation chamber that offers limited multipath control. We introduce a reconfigurable OTA chamber whose walls are lined with antennas, a few of which may be attached to a channel emulator and the balance of which are connected to reconfigurable impedances. Initial simulations and measurements with this topology demonstrate that through control of the impedances and the port excitations, the chamber offers significant control over the achieved fading distribution, spatial correlation, and power angular spectrum at the device under test.**

Keywords—MIMO systems; antenna measurements; over-the-air device testing

I. Introduction

As wireless device designs increasingly exploit multiple electromagnetic polarizations and propagation spatial degrees of freedom, the challenge of testing device performance in realistic and repeatable environments becomes increasingly difficult. This realization has motivated development of over-the-air (OTA) testing systems that measure the performance of complete end-to-end communications in a controlled propagation environment. Multi-antenna OTA testing [1, 2] surrounds the device under test (DUT) with an array of antennas, each connected to a channel emulator, in an anechoic chamber. While this technique offers channel synthesis flexibility, it can be expensive and complex. Mode-stirred reverberation chambers [3, 4] offer more economical testing, although the ability to control the detailed propagation parameters is limited.

Motivated by these observations, we introduce a reverberation chamber whose walls are lined with antennas, a small number of which are connected to transmitting sources and the remainder of which are connected to reconfigurable impedance elements (REs) [5]. Simulations of a two-dimensional version of this *reconfigurable OTA chamber* (ROTAC) demonstrate that controlling the statistics of the RE impedances enables control over the emulated fading distribution, spatial correlation, and power angular spectrum (PAS) observed at the DUT [5]. Measurements from a functional prototype ROTAC experimentally confirm that the technique has the potential to provide flexible, low-cost OTA testing.

II. Two-Dimensional Simulations

A. Chamber Model

Simulations represent an effective way to determine the potential ROTAC performance. This work considers a circular two-dimensional chamber for simplicity, although the simulation model can be extended to three-dimensional operation. The chamber model, depicted in Figure 1, consists of an outer wall whose surface is densely covered with radiating antennas that are accessible at external ports.

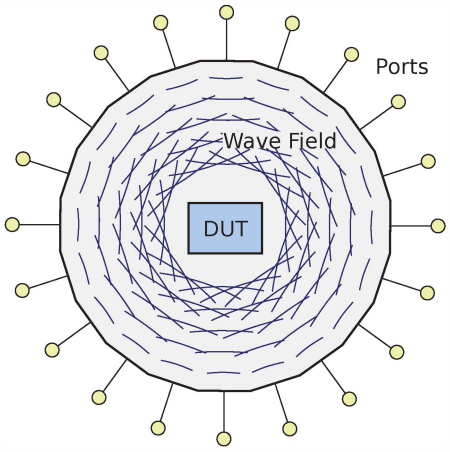

Fig. 1. Idealized two-dimensional chamber used for simulations of the ROTAC.

We model this chamber using a surface-based method of moments (MoM) framework [6] in which the TM_z fields in the chamber are completely determined by the z-polarized electric field $E_z(x, y)$ and its normal derivative $\partial E_z(x, y)/\partial n$ on the outer boundary. We define an equivalent voltage and current at each MoM basis function as E_z and $(1/jk_0\eta_0)\partial E_z/\partial n$, respectively, where k_0 and η_0 are respectively the wavenumber and intrinsic impedance of free space. This allows the chamber to be analyzed with equivalent circuit techniques, where the network parameters can be determined for the system and then network theory can be used to determine the system fields when a source or load is placed on the *terminal* of each basis function. Several adjacent basis functions are combined (either excited by the same source or terminated in the same impedance), with each set of combined basis functions representing a *port*.

B. Synthesis of Channel Fading

We consider a ROTAC with 32 ports and a diameter of 4λ, where λ is the free space wavelength. Four of the ports (spaced at 90° angular intervals) have active sources with constant voltage amplitude and phase, while the other 28 ports are ter-

978-1-4673-7441-5 /15/$31.00 ©2015 IEEE

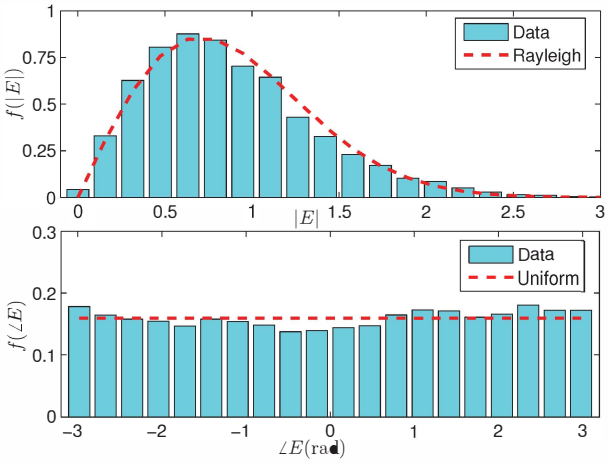

Fig. 2. Simulated amplitude and phase histograms of the field sampled at the center of the chamber for uniform random loads at the reconfigurable ports.

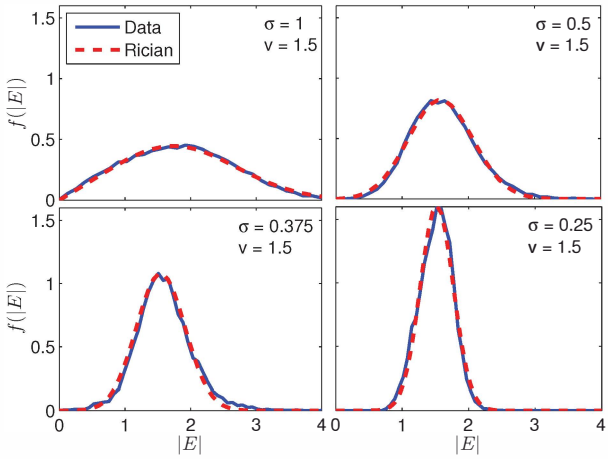

Fig. 3. Simulated amplitude pdfs of the field sampled at the center of the chamber for uniform RE reactances, where in each case the distribution parameters are optimized for a specific value of σ and ν.

minated with REs. To synthesize Rayleigh fading, the source voltages are $\mathbf{v}_s = [1,\ j,\ -1,\ -j]^T$, where $j = \sqrt{-1}$, and the source impedance is 377 Ω. The ith RE impedance is given by $Z_i = R_i + jX_i$, where $R_i = 34\ \Omega$, $X_i \sim \mathcal{U}(-500\ \Omega, 500\ \Omega)$, and $\mathcal{U}(x_1, x_2)$ denotes a uniform distribution on the interval $[x_1, x_2]$. Figure 2 plots the probability density functions (pdfs) of the amplitude $f(|E_z|)$ and phase $f(\angle E_z)$ of the field E_z at the center of the chamber obtained from 10^4 random reactance realizations. The statistics are close to that of an ideal Rayleigh distribution, and an analysis of the signal correlation as a function of antenna spacing shows that the correlation matches that expected for a rich multipath environment.

While achieving Rayleigh fading statistics demonstrates that the ROTAC can achieve the performance available from traditional mode-stirred reverberation chambers, the objective of the ROTAC is to enable more sophisticated fading distributions. We therefore pursue optimization of the following ROTAC parameters:

1) The source excitation voltage vector $\mathbf{v}_s$, whose elements can be arbitrary complex values (amplitude and phase) under the constraint $0 \le |v_{s,i}| \le 1$.
2) The resistance of the RE impedances ($R_i = R_0$) under the constraint $R_0 \in [10, 145]\ \Omega$.
3) The endpoints $X_{\min}$ and $X_{\max}$ of the uniform distribution used for the RE reactances, where $X_i \sim \mathcal{U}(X_{\min}, X_{\max})$. The bounds $X_{\min}, X_{\max} \in [-2\eta_0, 2\eta_0]$ and $X_{\min} < X_{\max}$ are assumed.

These parameters are collected into the 11-element vector

$$\mathbf{w} = [|\mathbf{v}_s^T|\ \angle\mathbf{v}_s^T\ R_0\ X_{\min}\ X_{\max}]^T, \tag{1}$$

where optimization of the parameters is performed using a genetic algorithm (GA) with a fitness function that minimizes the squared error between the ideal and realized fading pdfs.

The GA randomly creates an initial population of 100 vectors $\mathbf{w}$ and retains the $N_{\rm B} = 10$ vectors that achieve the best fitness. These $N_{\rm B}$ vectors are then used to generate $N_{\rm GA} = 60$ new population vectors using mutations and cross-overs, where cross-overs are only possible within the same parameter type (e.g. source voltages with source voltages) and the mutation probability is varied from 10% to 50%. The $N_{\rm B}$ vectors achieving the best fitness are retained, and the procedure is repeated 100 times, with the vector in the final population having the best fitness being chosen as the solution.

To demonstrate the performance of this approach, we synthesize a Rician distribution for $\xi = |E_z|$ given by

$$f(\xi|\nu,\sigma) = \frac{\xi}{\sigma^2}\exp\left[-\frac{(\xi^2+\nu^2)}{2\sigma^2}\right] I_0\left(\frac{\xi\nu}{\sigma^2}\right), \tag{2}$$

where I_0 is the zeroth-order modified Bessel function of the first kind. In our simulations, we optimize the impedance parameters for four different values of σ with $\nu = 1.5$. For fitness computations, we construct the histogram of E_z for each vector $\mathbf{w}$ using 10^4 random realizations of the reconfigurable impedances. Figure 3 plots the Rician pdf from (2) and the histogram for the chamber parameters generated from the GA, where the field is sampled at the chamber center. As can be seen, a very close fit to the desired distribution can be obtained by proper selection of the impedance parameters.

C. Directional Propagation Characteristics

Another objective of the ROTAC is to generate multipath fields with a specified PAS. To explore this possibility, the field strength as a function of propagation direction in the test region of the chamber is computed using

$$S(\phi) = \int_A E_z(x,y)\exp[-jk_0(x\cos\phi + y\sin\phi)]\ dA, \tag{3}$$

where the integral is performed over the circular area A of diameter $\lambda/3$ placed at the chamber center.

To obtain a desired PAS, we select the source voltages as $\mathbf{v}_s = [1,\ j,\ -1,\ -j]^T$ and termination resistances as $R_i = R_0 = 37\ \Omega$. We generate a set of 100 pairs of $(X_{\min}, X_{\max})$ with $X_{\min} \sim \mathcal{U}(-2\eta_0, 2\eta_0)$ and $X_{\max} \sim \mathcal{U}(X_{\min}, 2\eta_0)$. For each pair, 10^4 realizations of the impedances are generated, where $X_i \sim \mathcal{U}(X_{\min}, X_{\max})$, resulting in a library of 10^6

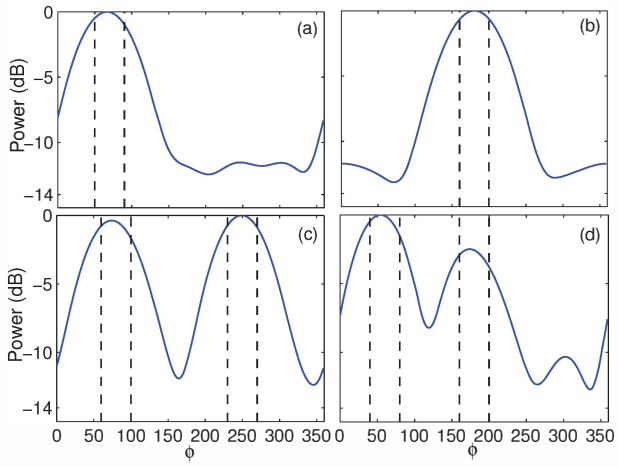

Fig. 4. Dependence of propagating power versus arrival angle ϕ generated for various desired directional profiles. Dashed lines bound the sectors where incident power is desired.

random solutions. The 10^3 solutions from the library whose function $S(\phi)$ best matches the desired PAS are retained.

Figure 4 illustrates the PAS produced by the best 10^3 solutions for four different PAS specifications, where the dashed lines bound the angular region where the average power is specified (target power outside these regions is zero). This simple example illustrates that even without detailed optimization, useful directional properties of the wave field can be controlled.

III. Experimental Validation

Figure 5(a) depicts an initial prototype ROTAC, which is a cube formed from five panels that are 11 inches square. Each panel, an example of which is shown in Figure 5(b), hosts a 3×3 grid of dual-polarization patch elements (resonant frequency 2.53 GHz, bandwidth 80 MHz) separated by $\lambda/2$. The cube is placed on a ground plane that is perforated with a grid of small holes that allow cable access to a DUT within the chamber, as shown in Figure 5(c).

The ports on each of the five panels provide a total of 90 ports that can be connected either to RF sources (*feed ports*) or REs or left unterminated (open circuit). The reconfigurable impedance used [7] enables a reflection coefficient phase tuning range of 200° with a maximum power loss of 3 dB over a bias range of 0-5 V.

A. Channel Fading

Measurements are performed using an 8×8 multiple-input multiple-output channel sounder [8], where four sounder transmit ports are connected to the vertical polarization port of the center antenna on each of the four side panels and a single sounder receive port is connected to a monopole in the middle of the chamber above the ground plane. An FPGA-controlled D/A sets the bias voltages applied to reconfigurable impedances connected to the vertical polarization ports of the antennas at the four corners of the side panels. The transmit RF signal consists of four tones separated by 5 MHz and centered at 2.53 GHz. Because the sounder activates one transmit port at

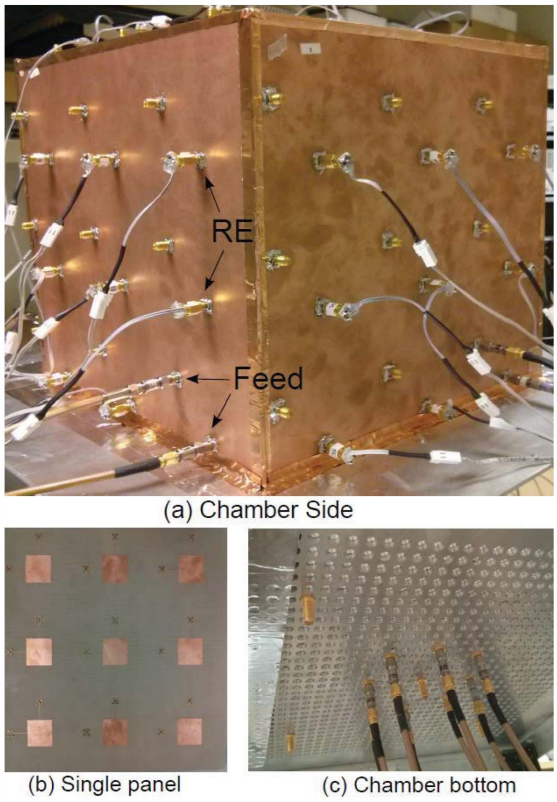

Fig. 5. Prototype ROTAC: (a) Side view of the complete chamber showing representative feed and RE ports; (b) A single chamber panel hosting the 3×3 grid of dual-polarized square patch antennas; (c) Bottom view of the chamber showing the RF cables that connect to an eight-element circular array of receiving monopole antennas.

a time, it measures the transfer function $\tilde{h}_\ell[n]$ from the ℓth feed port to the receive port at the nth frequency. Measurements of the four transfer functions, $1 \le \ell \le 4$, are captured for 10^6 different combinations of random impedance states (bias voltages). If the phase of the signal transmitted from the ℓth feed port is θ_ℓ, the realized channel response from the transmitter to the DUT at the nth frequency is

$$h_{\mathrm{R}}[n] = \sum_{\ell=1}^{4} \tilde{h}_\ell[n] e^{j\theta_\ell}. \tag{4}$$

Based on the measured data and (4), we perform a brute-force optimization where we realize 10^4 random phase combinations and then determine the single phase combination that produces channel responses whose magnitude and phase distributions are approximately Rayleigh and uniform, respectively. While not shown, this achieves an excellent match to a Rayleigh fading distribution. To achieve Rician fading, we fix the phases at $\theta_\ell = 0$ and select a subset of the impedance states that achieves the desired field amplitude distributions. Figure 6 shows the pdfs for these results for different target Rician distributions, verifying that the ROTAC is capable of providing a range of different fading distributions.

B. Directional Propagation Characteristics

We finally feed the horizontal polarization port of the antenna at the lower right corner of each side panel with an

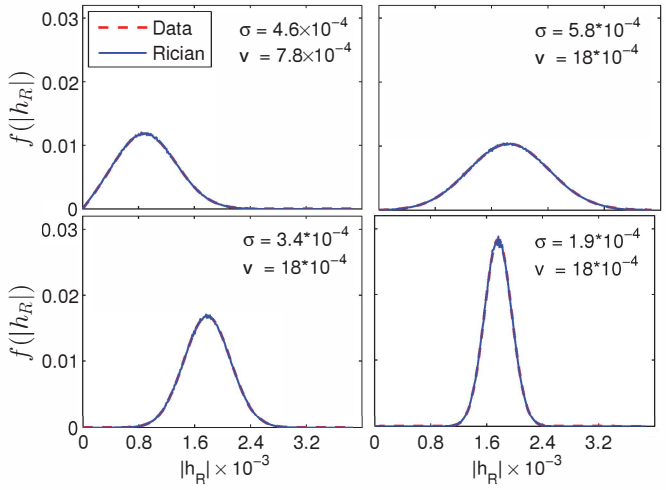

Fig. 6. Measured amplitude pdfs of the field sampled at the DUT antenna in the ROTAC compared to different Rician distributions, where σ and v control the Rician statistics.

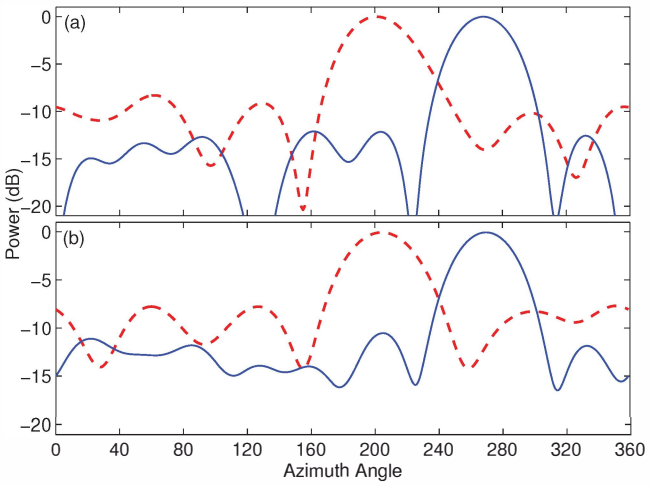

Fig. 7. Measured power incident on the DUT as a function of azimuth arrival angle for sources on the horizontal polarization port at the lower right corner of each face: (a) Single RE state; (b) Average over 50 RE states.

independent source and terminate the vertical polarization port of the remaining eight antennas on each panel (including the top panel) with a tunable impedance. We measure the fields inside the chamber using an array of eight monopole antennas arranged in a circle of radius $\lambda/2$ at the chamber center (Figure 5(c)). Let $\hat{h}_{k\ell}[n]$ represent the transfer coefficient from the ℓth transmit to the kth receive antenna at the nth frequency for one set of RE bias voltages (state). The signal at the kth receive antenna for this frequency is

$$h_k[n] = \sum_{\ell=1}^{4} a_\ell e^{j\theta_\ell} \hat{h}_{k\ell}[n] \tag{5}$$

where $a_\ell e^{j\theta_\ell}$ is the complex gain applied to the ℓth feed port signal and normalized such that $\sum_\ell a_\ell = 1$. The measurement record includes channels for 10^4 different RE states.

For each reconfigurable impedance state, we apply a randomly-chosen set of 10^4 complex gains $a_\ell e^{j\theta_\ell}$ and use the Bartlett beamformer on the circular array to estimate the PAS. For each gain combination, we find the peak of the PAS and define the sidelobe level (SLL) as the peak power observed at angles beyond the array beamwidth, which is the angular range between PAS first nulls for an incident plane wave. For each gain combination, we store the SLL for each state as well as the SLL averaged over the 50 states that achieve the lowest SLL for that gain.

Figure 7 plots the realized azimuth PAS, where the solid and dashed lines depict the results for the gains producing the lowest and highest SLL and the top and bottom plots show results when we look at the SLL for each state and averaged over the best 50 states, respectively. The results demonstrate that 1) the SLL depends on the desired arrival angle and 2) the SLL is only marginally higher for the averaged results, meaning that a single excitation can be effective for multiple different RE states. Most importantly, the data verifies that the ROTAC offers considerable control over the PAS, motivating development of more sophisticated optimization approaches.

IV. Conclusion

This paper reports on simulations and measurements demonstrating that a ROTAC can be used to generate specified fading statistics and angular field characteristics at the DUT by controlling the impedance of the REs along with the excitation applied to a few transmit ports. The results demonstrate that the ROTAC can potentially offer high emulated field control at a relatively low cost.

Acknowledgement

This work was supported in part by the U. S. Army Research Office under Grant # W911NF-12-1-0469.

References

[1] P. Kyösti, J.-P Nuutinen, and T. Jamsa, "MIMO OTA test concept with experimental and simulated verification," in *Proc. 4th European Conference Antennas and Propagation (EuCAP)*, Barcelona, Spain, Apr. 12-16, 2010, pp. 1–5.

[2] W. Fan, X. C. B. de Lisbona, F. Sun, J. O. Nielsen, M. B. Knudsen, and G. F. Pedersen, "Emulating spatial characteristics of MIMO channels for OTA testing," *IEEE Transactions on Antennas and Propagation*, vol. 61, no. 8, pp. 4306–4314, 2013.

[3] P-S. Kildal, C. Orlenius, and J. Carlsson, "OTA testing in multipath of antennas and wireless devices with MIMO and OFDM," *Proceedings of the IEEE*, vol. 100, no. 7, pp. 2145–2157, 2012.

[4] M. A. Garcia-Fernandez, J. D. Sanchez-Heredia, A. M. Martinez-Gonzalez, D. A. Sanchez-Hernandez, and J. F. Valenzuela-Valdes, "Advances in mode-stirred reverberation chambers for wireless communication performance evaluation," *IEEE Communications Magazine*, vol. 49, no. 7, pp. 140–147, 2011.

[5] J. W. Wallace, R. Mehmood, and M. A. Jensen, "Electronically reconfigurable reverberation chambers," in *Proc. 8th European Conference Antennas and Propagation (EuCAP)*, The Hague, The Netherlands, Apr. 6-11, 2014, pp. 3669–3673.

[6] A. M. Eid and J. W. Wallace, "Accurate modeling of body area network channels using surface-based method of moments," *IEEE Transactions on Antennas and Propagation*, vol. 59, no. 8, pp. 3022–3030, 2011.

[7] R. Mehmood, J. W. Wallace, and M. A. Jensen, "Key establishment employing reconfigurable antennas: Impact of antenna complexity," *IEEE Transactions on Wireless Communications*, vol. 13, no. 11, pp. 6300–6310, 2014.

[8] B. T. Maharaj, J. W. Wallace, M. A. Jensen, and L. P. Linde, "A low-cost open-hardware wideband multiple-input–multiple-output (MIMO) wireless channel sounder," *IEEE Transactions on Instrumentation and Measurement*, vol. 57, no. 10, pp. 2283–2289, 2008.